Formation of vacancy clusters and cavities in He-implanted silicon studied by slow-positron annihilation spectroscopy

Roberto S. Brusa,* Grzegorz P. Karwasz, Nadia Tiengo, and Antonio Zecca
Istituto Nazionale per la Fisica della Materia, Dipartimento di Fisica, Universita' di Trento, I-38050 Povo, Trento, Italy

Federico Corni, Rita Tonini, and Gianpiero Ottaviani
Istituto Nazionale per la Fisica della Materia, Dipartimento di Fisica, Universita' di Modena, I-41100 Modena, Italy
(Received 20 January 1999; revised manuscript received 14 June 1999)

The depth profile of open volume defects has been measured in Si implanted with He at an energy of 20 keV, by means of a slow-positron beam and the Doppler broadening technique. The evolution of defect distributions has been studied as a function of isochronal annealing in two series of samples implanted at the fluence of 5×10^{15} and 2×10^{16} He cm^{-2}. A fitting procedure has been applied to the experimental data to extract a positron parameter characterizing each open volume defect. The defects have been identified by comparing this parameter with recent theoretical calculations. In as-implanted samples the major part of vacancies and divacancies produced by implantation is passivated by the presence of He. The mean depth of defects as seen by the positron annihilation technique is about five times less than the helium projected range. During the successive isochronal annealing the number of positron traps decreases, then increases and finally, at the highest annealing temperatures, disappears only in the samples implanted at the lowest fluence. A minimum of open volume defects is reached at the annealing temperature of 250 °C in both series. The increase of open volume defects at temperatures higher than 250 °C is due to the appearance of vacancy clusters of increasing size, with a mean depth distribution that moves towards the He projected range. The appearance of vacancy clusters is strictly related to the out diffusion of He. In the samples implanted at 5×10^{15} cm^{-2} the vacancy clusters are mainly four vacancy agglomerates stabilized by He related defects. They disappear starting from an annealing temperature of 700 °C. In the samples implanted at 2×10^{16} cm^{-2} and annealed at 850–900 °C the vacancy clusters disappear and only a distribution of cavities centered around the He projected range remains. The role of vacancies in the formation of He clusters, which evolve in bubble and then in cavities, is discussed.

I. INTRODUCTION

Positron annihilation spectroscopy (PAS) performed with slow positron beams is a powerful and well-established technique to probe open-volume-defect profiles in solids.[1] Positrons, in fact, are efficiently trapped by open volume and negatively charged defects. PAS was used to investigate extensively the formation, the evolution and the electronic structure of defects in elemental and compound semiconductors.[2,3] In particular in the Doppler broadening experiments with positron beams the one-dimensional momentum distribution of the positron-electron annihilating pairs is measured. A narrowing of the momentum distribution is an index of positron trapping in vacancies and vacancy cluster defects.

Griffioen *et al*.[4] and Evans *et al*.[5] have found that nanocavities can be produced in Si by He implantation and subsequent thermal annealing of the samples. These authors showed that He implanted at high doses (2×10^{17} cm^{-2} fluence, 10 keV energy) coalesces in bubbles. Then, after annealing at temperatures higher than 800 °C, outdiffuses leaving empty voids. The dimensions of these voids are in the nanometer range. Recently there was a novel interest in void formation for scientific as well as for technological reasons. The optical[6] and electrical[7] properties and the surface energy[8] of these nanostructures were investigated. The clean cavity walls of these voids were used to determine the bond strength of H on Si.[9] Voids formed by He implantation in Si were demonstrated to be good centers for gathering metal contaminants.[10,11] This last finding could open new methods to confine these contaminants that are known to reduce the performances and the reproducibility of semiconductor devices produced by the very large scale integration. It was also found that[10] cavities can be only formed if a local concentration of 3.5×10^{20} He cm^{-3} is reached in the sample.

Although the recipe to obtain cavities by ion implantation with He is well known, the fundamental mechanisms that bring about their formation are not yet well understood. One of the remaining questions is related to the role of the open volume defects of atomic scale (vacancies and vacancy clusters) in cavities formation and to their interaction with the implanted helium. It must be stressed that in the works cited above, cavities are considered those open volume defects with the minimum dimension that is resolved by transmission electron microscopy (TEM) measurements. This means that cavity dimensions range from a few nanometers to hundreds of nanometers. For this reason, to our knowledge, no detailed studies were done on Si-implanted He at low fluence, where only smaller voids are formed. On the other hand, the PAS technique is very sensitive to open volume defects from atomic dimensions, and opens new possibilities in understanding the He-vacancy interaction at the threshold of the He fluence necessary to obtain cavities.

In a previous paper we have investigated the first stages of

 ©2000 The American Physical Society

open-volume-defects formation (vacancies and divacancies) in samples implanted at two doses and annealed isothermally at 250 °C.[12] The temperature at which He starts to outdiffuse from our samples is 250 °C.

For this work we have measured by PAS two series of samples. The first one implanted at He dose (5×10^{15} cm^{-2}, 20-keV-He energy) below the threshold for cavities formation. The second one implanted at a He dose just above the threshold for cavities formation (2×10^{16} cm^{-2}, 20-keV-He energy). The samples of the two series were isochronally annealed from 150 to 900 °C in order to study the evolution of the open-volume-defect profiles. To get information about the evolution of He and displaced Si atom distributions, similar samples were also characterized with Rutheford backscattering in channelling (RBSC), elastic recoil detection analysis (ERD),[13] and thermal programmed desorption (TPD) measurements.[14] TEM was performed to identify the nanostructures.

The paper is organized as follows. In Sec. II we give the details about the sample preparation, their thermal treatments, and the slow-positron measurements. We also report briefly some information about the techniques (RBSC, ERD, TEM, TPD) employed to characterize the samples. A brief summary of the experimental results obtained by RBSC, ERD, TEM, TPD measurements are presented in Sec. III. In Sec. IV the analysis of PAS measurements is presented and an attempt is made to identify the nature of the open volume defects as seen by PAS. It is known that the identification of defects in Doppler-broadening measurements has been an unresolved problem for years. An important step in this direction has been made in the theoretical work of Hakala *et al.*[15] In this section we present the first experimental evidence in favor of this identification. In the last part of Sec. IV the evolution of the open volume defects is described. Section V is devoted to the discussion of the interaction of the different type of defects and their role in the formation of cavities. All the details of the mathematical analysis of the PAS measurements needed to extract information about the defects distribution, the defects concentration and the characteristic positronic parameters that identify the defects are left to the Appendix.

II. EXPERIMENT

A. Samples

Two series of samples were obtained from high-purity *p*-type (1.7–2.5 Ω cm) silicon wafers, Czochralski-grown, (100) oriented. The samples were implanted at 20 keV with He fluence of 5×10^{15} and 2×10^{16} cm^{-2} (low dose, LD and high dose, HD, respectively), at a beam current density of about 8 $\mu A\,cm^{-2}$. The sample holder was kept at liquid-nitrogen temperature (LNT) during the implantation process and the samples tilted by 7° to avoid ion channeling. One sample implanted at room temperature (RT) with a He fluence of 5×10^{15} cm^{-2} has been measured in order to allow a comparison with LNT results. The 20-keV implantation energy was chosen in order to implant He deeply enough to ensure that He does not effuse during implantation and storage at room temperature. The He implantation profile was simulated by SRIM98 code.[16] At 20 keV implantation energy the He-projected range R_p was found to be about 235 nm with a straggling ΔR_p of 85 nm. The simulation by SRIM98 code also gives the vacancies distribution due to implantation, centered around 175 nm. It must be stressed that the SRIM98 code does not take into account the recombination process between displaced atoms and vacancies or clustering of vacancies and of helium atoms during implantation. Samples of both implantation doses were isochronally annealed in a 10^{-5} Pa vacuum for 2 h in the 150–900 °C temperature range at steps of 50°.

B. PAS measurements

To identify the open-volume-defects distributions in the two series of samples we have performed Doppler-broadening measurements of the positron annihilation line with an electrostatic positron beam coupled with a high-purity germanium detector. The resolution of the detector measured at the 356-keV line of Ba^{133} was 1 keV with 6-μs shaping time in the spectroscopy amplifier. Details about the apparatus are reported in Refs. 17,18. More information about the Doppler-broadening technique, used in particular for the defects characterizations in Si, can be found in Refs. 2,19. In PAS, with the Doppler-broadening technique, the shape of the 511-keV annihilation line is characterized by the so-called S parameter. The S parameter is calculated as the ratio of the counts in the central area of the peak ($|511-E_\gamma|\leqslant0.85$ keV) and the total area of the peak ($|511-E_\gamma|\leqslant4.25$ keV). Our choice of the energy windows is reported in parenthesis. The Doppler broadening of the 511-keV annihilation line ΔE is related to the electron-positron annihilating pair momentum component p_z, in the detector direction, by the relation $E=p_zc/2$. The S parameter reflects the fraction of positron annihilating with electrons of low momentum. In particular our energy window corresponds to momentum in the $0\leqslant p_z\leqslant3.3\times10^3 m_oc$ range. In our analysis of PAS data we have also utilized the wing parameter W that is the relative fraction of the counts in the wings region of the annihilation line. The windows chosen for the wings were $1.6\leqslant|E_\gamma-511|\leqslant4.0$ keV corresponding to positrons annihilating with high-momentum electrons $6.2\times10^{-3}m_oc\leqslant p_z\leqslant15.6\times10^{-3}m_oc$. The S and W parameters were measured as a function of the positron implantation energy in the 0.06–25 keV energy range. In silicon this corresponds to a mean positron implantation depth ranging from 0.13 nm to 3.5 μm. The Doppler-broadening spectra were acquired with microspectra methods and stabilized by a software procedure.[20] At each positron implantation energy, 3×10^5 counts in the 511-keV annihilation line were accumulated. This corresponds to a statistical error of 0.1% on the measured S parameter.

C. RBSC, ERD, TEM, TPD measurements

Several techniques were performed on a series of samples similar to those used for PAS measurements. The distribution of equivalent displaced silicon atoms was measured by RBSC with a 2-MeV $^4He^+$ beam aligned to the [100] crystal direction. The ions were collected with two detectors placed at 160° and 120° scattering angles. The distribution of He contents was investigated by ERD, using a $^{15}N^{++}$ beam at 7 and 8 MeV. The samples were tilted 75° and the detector

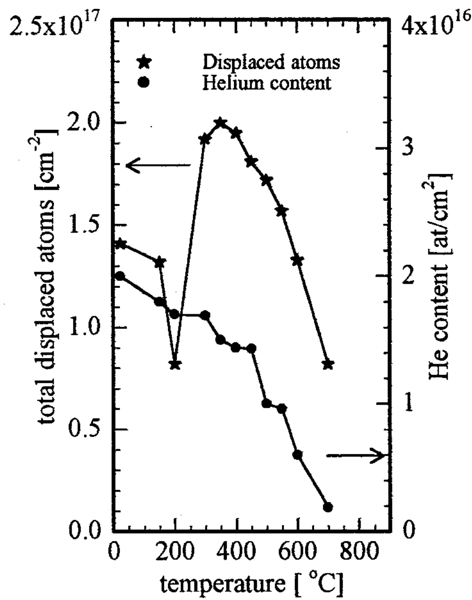

FIG. 1. Displaced silicon atoms as measured by RBSC, and He fluence as measured by ERD, as a function of the annealing temperature, for the samples implanted at 2×10^{16} He cm^{-2}.

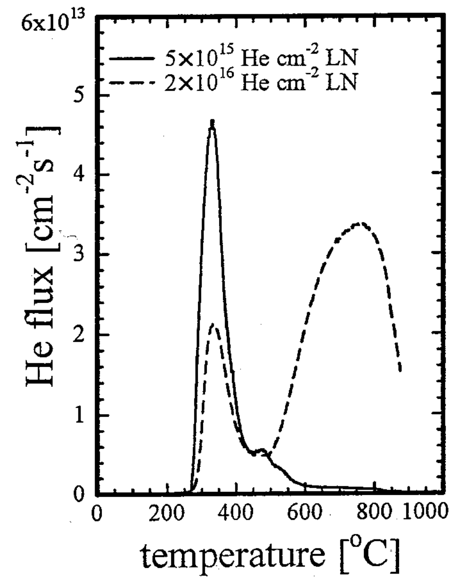

FIG. 2. Thermal desorption spectra (heating rate of 45 °C min^{-1}) for the as-implanted samples at LD (full line) and HD (broken line).

placed at 30°. A mylar film 6 μm thick placed in front of the detector suppressed the scattered nitrogen beam. TEM analysis was made on selected cross-sectioned samples using a Philips EM400 microscope. TPD measurements give the desorption rate of He (amount of He leaving the unit surface per unit time). Information about the activation energies can be extracted from the desorption rate. Moreover, the integral in the time of the desorption rate gives the total amount of He released. TPD spectra were collected for the as-implanted samples of the two investigated doses.

III. RBSC, ERD, TEM, TPD: EXPERIMENTAL RESULTS

For a detailed description and discussion of the RBSC, ERD, TEM, TPD measurements and results we refer the reader to Refs. 13,14,21. Here we only resume the main results obtained with these techniques; these results will be useful in the following PAS data description and discussion.

The total number of equivalent displaced silicon atoms in the series of samples implanted at 2×10^{16} He cm^{-2} is shown in Fig. 1, as extracted from RBSC measurements. The distribution of displaced silicon atoms in the as-implanted samples extends from the surface down to 230 nm, with a mean depth of about 130 nm. In the samples annealed up to 200 °C there is a recovery of the damage in the first 170 nm. After annealing at 250 °C, a new damage appears at a depth of about 180 nm. From 250 °C the mean position of the distribution remains unchanged. At 350 °C this new damage has a quite symmetric distribution with a full width at half maximum of 60 nm. The concentration of displaced silicon atoms is about constant in the 350–500 °C annealing range. From 500 °C to 800 °C it decreases monotonically and finally disappears.

The total He contents measured by ERD for the samples implanted at 2×10^{16} He cm^{-2} is presented in Fig. 1 as a function of the annealing temperature. In the as-implanted sample the He distribution extends from the surface down to 400 nm with a mean depth of 220 nm. The mean depth of the He distribution does not change during the isochronal annealing, and remains symmetric. After annealing up to 250 °C the quantity of He in the samples is almost the same but the distribution is narrower: at 350 °C the full width at half maximum is about 80 nm. Annealing up to 400 °C leads to a moderate loss of He (less than one-third of the initial contents). At higher temperatures the loss is more rapid: almost all He outdiffuses in the 2 h annealing at 700 °C.

Measurements on samples implanted at 5×10^{15} He cm^{-2} have shown that the He distribution was centered around 220 nm; this mean depth moved to 170 nm after annealing at 250 °C.[21] At 250 °C the helium amount was about 2×10^{15} cm^{-2} and the displaced silicon atoms about 6×10^{15} cm^{-2}. In the LD samples annealed at a temperature higher than 250 °C, RBSC and ERD measurements were below the limit of their sensitivity.

TEM analysis was not able to detect any defect in the LD samples. On the contrary, defects were visible in the HD samples. At 400°C the damage shows a band 80 nm wide at a mean depth of 210 nm. These defects, with an electron optical density lower than the matrix, were identified as nanoagglomerates stabilized by He atoms. Small voids were observed in the tail of the damaged region towards the surface. After annealing at 700 and 900 °C, cavities appeared in this damaged region (70 nm wide, always centered at 210 nm). The density of these cavities was estimated to be 10^{10} and 10^{9} cm^{-2} for the two annealing temperatures, respectively. The cavities in the sample annealed at 700 °C have a mean diameter of 11 nm. The cavities after annealing at 900 °C reach a shape with well-defined facets[22] with a mean diameter of 15 nm.

TPD measurements were performed at a constant heating rate. In Fig. 2 the TPD spectra, obtained at a heating rate of 45 °C min^{-1} for the as-implanted samples of the two inves-

tigated doses are shown. The helium release starts at 250 °C. Both samples present a peak in the desorption rate around 350 °C. In the sample implanted at the low He dose, the desorption rate decreases reaching zero at 600°C. On the contrary, the sample implanted at the high He dose presents a minimum between 400 and 500 °C and a second large peak with a maximum at 750 °C. The decrease of the desorption rate in the 350–500 °C range is well in agreement with the ERD results in Fig. 1: in fact the He contents as measured by ERD is about constant in the same temperature range. The analysis of TPD measurements[14] has pointed out that implanted helium is spatially distributed in agglomerates of different sizes. The He activation energy has a continuous distribution ranging from a minimum of 1.17 eV to a maximum of 1.7 eV. This last value was attributed to detrapping of He atoms from the largest nanoagglomerates.[4] On the other hand, the cavities, as seen by TEM measurements, are only present in the 2×10^{16} He cm^{-2} implanted samples annealed at temperatures higher than 650 °C. Figure 2 confirms qualitatively that He is bound in a different way in the samples implanted at the two doses. In the LD sample all He atoms are desorbed below 600 °C. In the sample implanted at the dose above the critical concentration for bubbles formation (2×10^{16} He cm^{-2}), more He desorbs at temperatures higher than 600°C. This is an indication that He is detrapped from large agglomerates. The peak of desorption is reached close to 700 °C, where the first cavities appear.

IV. PAS

A. Analysis of the experimental results

In Fig. 3 we show selected S-parameter measurements, normalized to the silicon S bulk value, as a function of positron implantation energy. A sample implanted at 5×10^{15} He cm^{-2} and annealed at 900 °C was adopted as the reference sample. The choice of the reference sample in Doppler-broadening PAS is a nontrivial task: our choice is explained in the Appendix. The S parameter of the reference sample starts from a low surface S value and increases monotonically towards the bulk S value. This behavior reflects the backdiffusion of the implanted positrons toward the surface.[2] In the as-implanted sample, and in the sample implanted and annealed at 450 °C, the S parameter reaches a maximum before decreasing to the S bulk value. The difference of the S parameter of these samples with respect to the reference sample indicates that more positrons annihilate with electrons of low momentum: this difference is related[2,19,23] to positrons trapped in open volume defects. The fact that at positron implantation energies higher than 18 keV the S parameter converges to the bulk value means that positrons with these energies are implanted much deeper than the defected region.

Every type of open volume defect is characterized by a typical S_d parameter. The PAS data were analyzed by best fitting the S vs E curves with the diffusion equation describing the positron motion in the steady state.[23] With this model, giving as input an estimate for the defect profile, it is possible to obtain for every S vs E spectrum an S_d value. If more than one defect is present in the sample, the evaluated S_d represents a weighted value of the corresponding S_d's.

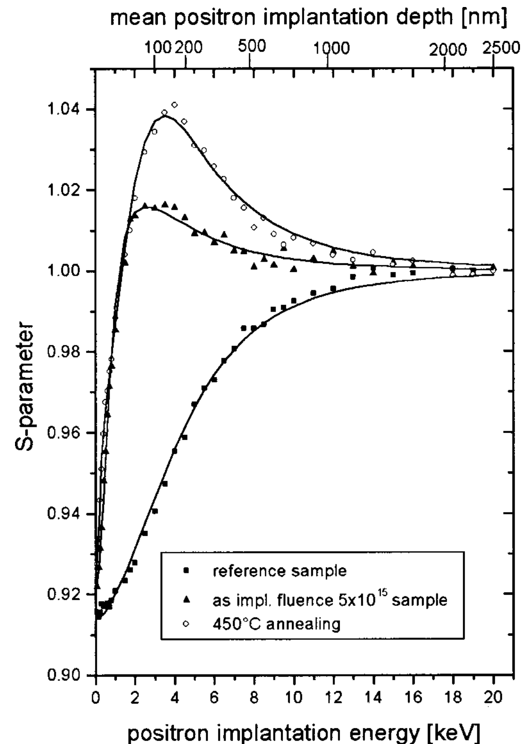

FIG. 3. S parameter of the Doppler-broadened annihilation line vs positron implantation energy: reference sample, full squares; LD sample implanted with He at 20 keV, full triangles; LD sample annealed at 450 °C, open circles. The lines through the experimental points are best fit curves obtained according to the diffusion model.

From our fitting procedure of the measured spectra the mean depth $\bar{d}$ of the defect profile and the specific trapping rate related to the defect concentration N_{nv} were also obtained. In a few cases where the diffusion equation analysis failed to give reliable values for S_d, we have used a different, complementary approach proposed by Clement *et al.*[24] This method allows us to determine the characteristic S_d and W_d values of the defected layer by studying the trajectory of the shape $S(E)$ and $W(E)$ parameters plotted in a S-W plane with the positron implantation energy as a running parameter. All the analysis details are discussed in the Appendix. The results are summarized in Table I for the two series of samples. The values of S_d as a function of the annealing temperature are different in the two series of samples. In the LD series S_d has a constant value of 1.02 up to 200 °C. In the 250–400 °C and 450–850 °C temperature range S_d has a value of 1.04 and 1.06 , respectively. In the HD series, S_d is constant (1.038) up to 400 °C, then increases progressively from 1.047 (450 °C) to 1.112 (700 °C). In a few cases two values for the mean depths are reported in Table I: this means that the defect profile is better described by two functions. This can be attributed to the coexistence of two distributions of defects centered at different depths. The guess profile adopted for the analysis of most S vs E measurements was the derivative of a Gaussian. Samples implanted at HD and annealed at 800,850,900 °C were analyzed using a Gaussian profile for this estimation. The full width at half maximum (FWHM) of such a Gaussian is reported in Table I.

TABLE I. Results of the fitting procedure applied to the S vs E data measured by PAS for LD and HD samples: characteristic S_d value of the defects, number of defects N_{nv} per unit surface, mean depths $\bar{d}_1$ and $\bar{d}_2$ of the defect density profiles. The error on N_{nv} is 30%; the error on $\bar{d}_1$ and $\bar{d}_2$ is 10%. The values reported in square brackets are only indicative.

	Samples implanted at a fluence of 5×10^{15} He cm^{-2}				Samples implanted at a fluence of 2×10^{16} He cm^{-2}				
Samples	S_d	$\bar{d}_1$ (nm)	$\bar{d}_2$ (nm)	$N_{nv}(\times10^{14})$ cm^{-2}	S_d	$\bar{d}_1$ (nm)	$\bar{d}_2$ (nm)	FWHM	$N_{nv}(\times10^{14})$ cm^{-2}
As-implanted	$1.02^{-0.002}_{+0.0022}$	31		$16.6V_1^*$	$1.0376^{-0.007}_{+0.009}$	44.4			$1.37V_2^*$
Annealing T (°C)									
150	1.02	28.8	4.44	$6.64V_1^*$	1.0376	53.2			$0.83V_2^*$
200	1.02	71	5.3	$2.5V_1^*$	1.0376	57.7			$0.4V_2^*$
250	$1.04^{-0.005}_{+0.014}$	53.2	3.55	$0.73V_2^*$	1.0376	64.3			$0.39V_2^*$
300	1.04	80	4.0	$1.40V_2^*$	1.0376	99.8			$0.18V_2^*$
350	1.04	86.5	3.55	$1.83V_2^*$	$1.038^{-0.006}_{+0.014}$	88.7			$2.07V_2^*$
400	1.04	88.7	3.1	$3.22V_2^*$	1.038	95.4			$2.50V_2^*$
450	$1.061^{-0.013}_{+0.022}$	84.2	2.2	$1.60V_4^*$	$1.047^{-0.01}_{+0.016}$	95.4			$3.12V_2^*$
500	$1.057^{-0.006}_{+0.015}$	91	2.7	$1.87V_4^*$	$1.052^{-0.003}_{+0.005}$	95.4			$1.38V_3^*$
550	$1.065^{-0.012}_{+0.03}$	75.4	2.2	$2.0V_4^*$	$1.0612^{-0.008}_{+0.005}$	104.2			$1.25V_4^*$
600	$1.063^{-0.012}_{+0.018}$	53.2	2.7	$1.77V_4^*$	$1.0877^{-0.013}_{+0.018}$	84.2	7.0		$0.52V_6^*$
650	1.063	55.0	2.0	$1.80V_4^*$					
700	few defects				$1.112^{-0.03}_{+0.06}$	93.2	7.0		$10^{-4}V_c$
750	[1.063]	[88]		$[0.023V_4^*]$	1.112	115.3	8.8		$0.75\times10^{-4}V_c$
800	[1.063]	[30]		$[0.07V_4^*]$	1.112	142		48 ± 10	$0.22\times10^{-4}V_c$
850	[1.063]	[97]		$[0.018V_4^*]$	1.112	232		48 ± 10	$0.17\times10^{-4}V_c$
900	no defects				1.112	235		35 ± 10	$10^{-5}V_c$

The continuous curves through the experimental points in Fig. 3 were obtained by applying the best fitting procedure cited above.

In the following, as in previous papers,[12] we present the data in a form that gives more direct information about positron trapping in open volume defects. With reference to Fig. 3, this information is contained in the difference of the S value of the given sample minus the S value of the reference sample. As the measured S values have been fitted we have rewritten them as $\tilde{S}=(S-S_s)/(S-S_b)$, where S_s is the S value at the surface as determined by the fitting procedure and $S_b=1$ is the bulk S value common to all samples. For the sake of having a less noisy reference, we have used the S values obtained through the fitting procedure on the reference sample as reference values and we have calculated $\tilde{S}^{fit}_{ref}$ with the above formula. For each sample the difference $\Delta S=\tilde{S}-\tilde{S}^{fit}_{ref}$ has been calculated and has been plotted as a function of the mean implantation depth. The mean positron implantation depth has been calculated from Eq. (A8) (see the Appendix). The ΔS values are related to the probability f_d of positrons to be trapped in a defect. The probability f_d is calculated through the diffusion equation and depends on the positron specific trapping rate per unit defect concentration [Eqs. (A4) and (A5) of the Appendix]. The PAS measurements and the fitting curves are shown in Figs. 4 and 5 as ΔS vs mean positron depth, for the isochronal annealing.

B. Identification of open volume defects

As reported in Table I the S_d values characterizing the type of positron traps are different in the two as-implanted samples and they change with the thermal treatment. Larger values of the S_d parameter are an index of larger open volume defects in silicon.[15]

Before discussing the results in Figs. 4 and 5, we have to identify the positron traps corresponding to the S_d values. For the sample implanted at HD and annealed in the 700–900 °C temperature range, the assignment is straightforward. In these samples cavities are seen by TEM, and we have assigned the value of $S_d=1.112$ to these defects. This value is in very good agreement with the value of 1.119 found by Hakvoort *et al.*[25] for stable voids obtained in implanted Si samples with 2.5 keV He at a dose of 1.6×10^{16} He cm^{-2} and annealed at 800 °C.

The values of S_d in the 1.034–1.038 range were assigned to divacancies[26,27] and $S_d=1.052\pm0.003$ to negatively charged divacancies[28] in Si. Only Avalos and Dannefaer[29] have reported a higher (1.067) value for neutral divacancies in a 10-MeV electron irradiated Fz silicon.

Recently Hakala *et al.*[15] have calculated positron lifetime and, for the first time, momentum distribution of electron-positron pairs annihilating at vacancy clusters in Si. In these calculation they have considered an ideal vacancy cluster in which the ions surrounding the defects are not allowed to relax from their ideal lattice position. From the calculated momentum distribution they have extracted the Doppler spectrum and convoluted it with an experimental resolution curve (a Gaussian with FWHM$=4.7\times10^{-3}m_oc$). From this Doppler spectrum they have calculated the S_d parameters for monovacancies V_1 to clusters of five vacancies V_5. In Fig. 6 we have reported our S_d values, obtained by fitting the PAS data, as a function of the annealing temperature for the two series of samples. On the same figure the S_d values calcu-

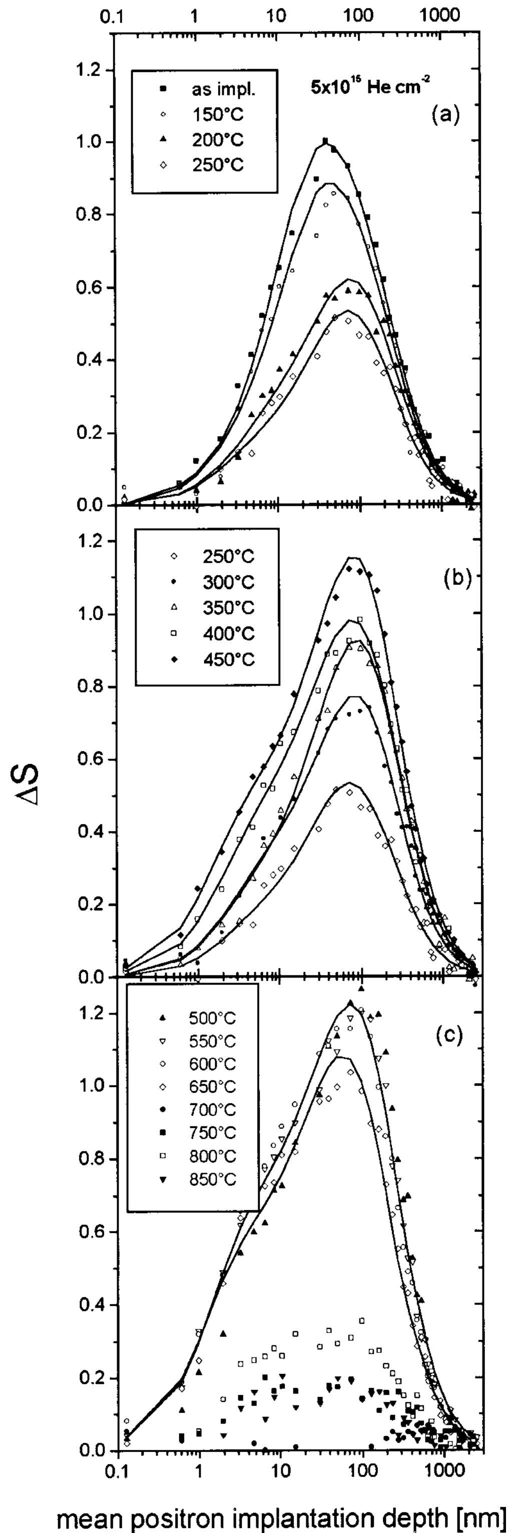

FIG. 4. ΔS (see text) vs mean positron implantation depth for LD samples. (a) As-implanted, fyull squares; 150 °C, open circles; 200 °C, full triangles; 250 °C, diamonds. (b) 250 °C, diamonds; 300 °C, full circles; 350 °C, open triangles; 400 °C, open squares; 450 °C, full diamonds. (c) 500 °C, full triangles; 550 °C inverted triangles; 600 °C, open circles; 650 °C, open diamonds; 700 °C, full circles; 750 °C, full squares; 800 °C, open squares; 850 °C, inverted full triangles. The lines through the experimental points are best fit curves obtained according to the diffusion model. (c) The best fits for 550 °C and 650 °C only are reported for clarity.

lated in Ref. 15 are reported as dotted lines; these lines are labeled on the right axis. The resolution function of our detector at 511 keV was $4.6\times10^{-3}m_oc$ FWHM, very close to the resolution function used in Ref. 15, and therefore we do not need any correction for the comparison of S_d values. Figure 6 deserves some comments.

(a) The calculated S_d values[15] are for ideal vacancies and vacancy clusters. In our samples, as will be shown, the open volume defects are stabilized by He or displaced Si-related defects. This is certainly the case of monovacancies in the LD sample; in fact it is well accepted that single vacancies are not stable at room temperature in Si.[30]

(b) In our samples there is certainly a distribution of different types of open volume defects. For example, in the sample implanted at 2×10^{16} He cm^{-2} and annealed at 700 °C, TEM measurements have shown cavities in a region 70 nm wide centered at 210 nm, and this is in agreement with our finding, but positrons see also a well-defined distribution of defects from the surface up to this depth. These defects are smaller than cavities and are not seen by TEM. The heterogeneity of the open volume defects will also be reflected in our S_d values. These experimental values can be thought of as linear combination values coming from defects of different types. Also the values of 1.034–1.038 assigned to divacancies in previous works,[26–28] most probably reflect the coexistence of divacancies and monovacancies possibly stabilized by impurities. This coexistence was postulated in measurements on samples implanted with He and treated isothermally at 250 °C (Ref. 12) and would explain our values in some samples in Fig. 6 that lie between the calculated values for monovacancies and divacancies.

(c) The presence in our samples of negatively charged defects like V_2^{-1}, V_2^{-2} cannot be excluded.

(d) It cannot be excluded that positrons are also trapped in open volume defects partially filled by He atoms.

However, with the mentioned cautions, we have classified the defects in our samples according to Fig. 6 (see also Table I, columns five and ten). In the following we will use the term $V_1^*, \ldots, V_5^*$ helium-related defects (i.e., vacancy complexes stabilized by He or other impurities) to label a distribution of defects with a predominance of open volume defects with $V_1, \ldots, V_5$ character. This is the more general assumption but we must stress that our data points in Fig. 6 line up in horizontal lines. This suggests, for instance, that our V_2^* are mostly V_2 with an S_d value different but compatible with the one given by Hakala *et al.*[15]

In Table I we have reported the concentration of defects calculated through Eq. (A5) of the Appendix. With the hypothesis that the characteristic trapping rate ν_n for an agglomerate of n vacancies is proportional to the characteristic trapping rate ν_v of a neutral vacancy $\nu_n = n\nu_v$,[19,31] the number N_{nv} of defects per surface area per host atom was evaluated with the relation $\nu = N_{nv}\nu_v/N_{\rm Si}$, where $N_{\rm Si}$ is the number of silicon atoms per unit volume. As a characteristic trapping rate for a neutral vacancy we have used half of the value $\nu_{2v} = 0.8\times10^{15}$ s^{-1} for a neutral divacancy.[32] For cavities a trapping rate $\nu_c = 10^{19}$ s^{-1} was evaluated from Eq. (5) using the cavity density as estimated by TEM measurements (Sec. III).

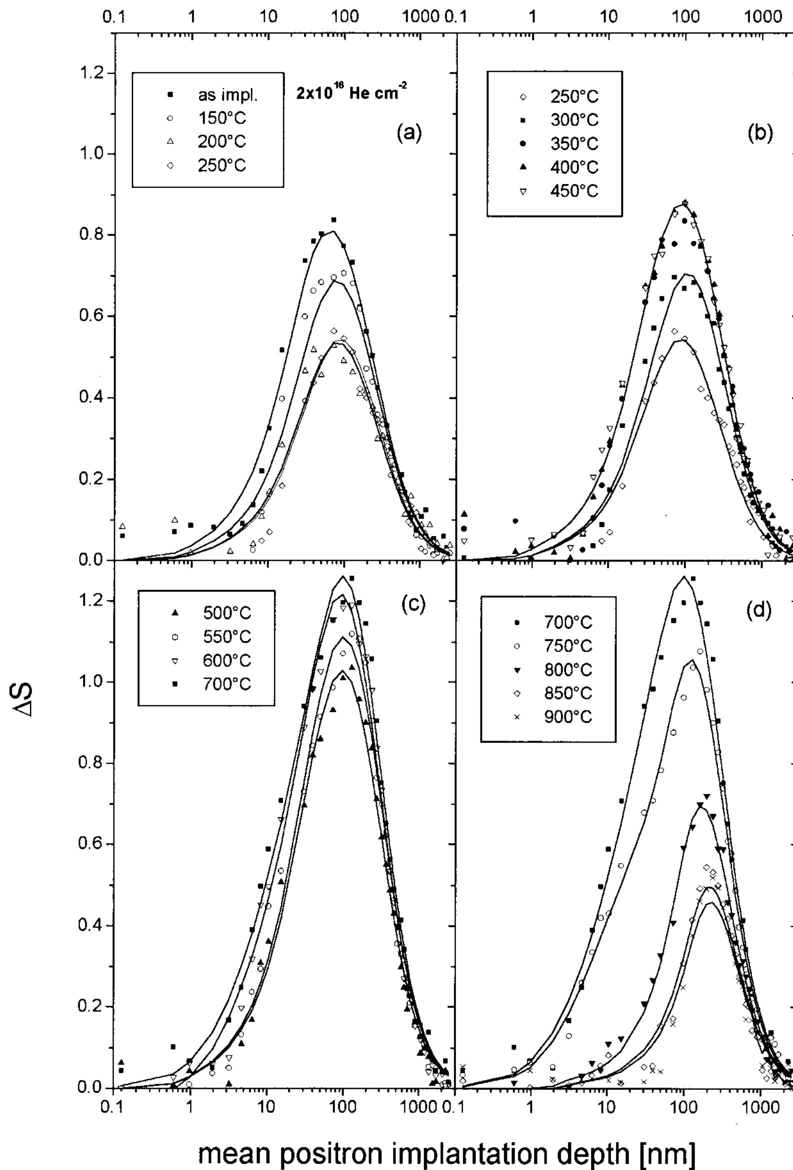

FIG. 5. ΔS (see text) vs mean positron implantation depth for HD samples. (a) As-implanted, full squares; 150 °C, open circles; 200 °C, triangles; 250 °C, diamonds. (b) 250 °C, diamonds; 300 °C, full squares; 350 °C, full circles; 400 °C, full triangles; 450 °C, inverted triangles. (c) 500 °C, full triangles; 550 °C open circles; 600 °C, inverted triangles; 700 °C full squares. (d) 700 °C, full squares; 750 °C, open circles; 800 °C, inverted triangles; 850 °C, diamonds; 900 °C, crosses. The lines through the experimental points are best fit curves obtained according to the diffusion model. The best fits for the 250 °C, 300 °C and 400 °C only are reported for clarity.

C. Evolution of the open volume defects

The evolution of the open volume defects as measured with PAS will be discussed with reference to Figs. 4, 5, and Table I.

1. As-implanted samples

In Figs. 4(a) and 5(a) the ΔS values vs the mean implantation depth of positrons are reported for the two as-implanted samples at LNT. A sample, not shown in the figures, implanted at LD and at RT, was also measured ($S_d = 1.02$, $N_{nv} = 4.2\times 10^{14} V_1^*$ cm^{-2}, $\bar{d}_1 = 22$ nm). All the implanted samples present a very near-to-the-surface positron trap distribution. The mean depth runs from about 44 nm in the sample implanted at the highest dose to 31 and 22 nm in the samples implanted at the lowest dose at LNT and RT, respectively. These traps are at a depth five times smaller than the mean depth of the He distribution (210 nm) and three times smaller than the mean depth of the displaced silicon atoms distribution (130 nm) as measured by RBSC. These observations have been interpreted as showing that the majority of vacancies produced during the implantation process is either passivated by He or involved in the formation of more complex defects.[12]

In the samples implanted at lower dose only V_1^* stabilized by He-related defects survives. Due to the increased mobility of both He and vacancies during the implantation process, the V_1^* concentration is lower in the sample implanted at RT. In the sample implanted at HD, the defects are mainly V_2^*. It is worth noting that the concentration of positron traps is lower by three and two orders of magnitude in comparison to displaced silicon atoms and He content, respectively. Positron traps are less numerous in the samples implanted at HD than in the samples implanted at LD.

2. Isochronal annealing of 5×10^{15} He cm^{-2} implanted samples

In the first two isochronal annealings (150,200 °C) we observe a considerable decrease of V_1^* traps. In the sample annealed at 150 °C the mean depth $\bar{d}_1$ of V_1^* distribution does not change with respect to the as-implanted sample. On the contrary, in the samples annealed at 200 °C the decrease V_1^*

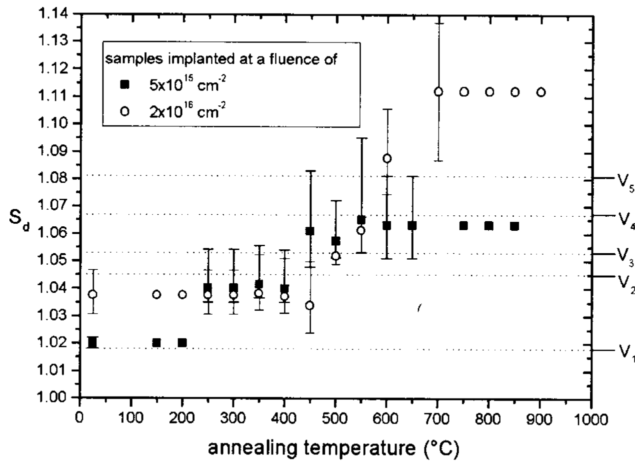

FIG. 6. Characteristic S_d parameters as a function of the annealing temperature for the samples implanted at LD and HD. The S_d values were obtained by the analysis described in the Appendix. The S_d values shown without error bars were kept fixed in the analysis with the diffusion equation. The dashed lines indicate the S_d values as calculated in Ref. [15] for the defects indicated on the right axis.

is accompanied with an increase of $\bar{d}_1$ and with a consequent broadening of the trap distribution. At 250 °C, V_2^* appear, and the minimum number of positron traps is reached.

The concentration of V_2^* increases monotonically up to 400 °C [Fig. 4(b)]. At 300 °C the mean depth $\bar{d}_1$ reaches the value of 80 nm. In the 300–450 °C temperature range $\bar{d}_1$ remains practically unchanged. From 450 to 650 °C, the positron traps are mainly V_4^*: their distribution at 600 and 650 °C [Fig. 4(c)] moves toward the surface (about 50 nm) and their number decreases.

In the 700–900 °C temperature range a nonmonotonic behavior of defects was detected [Fig. 4(c)]. In this temperature range we have measured two samples, produced in the same experimental condition, for every annealing temperature. All of them showed the same behavior. The positron traps in these samples are from 50 to 100 times less than in the other investigated samples. At 700 °C there is only a small deviation from the reference sample near 200 nm. At 750 and 800 °C there is an increase of positron traps with a broad distribution. At 850 °C they decrease again. At 900 °C all the positron traps are annealed out. The measured S-parameter values for the samples in the 700–850 °C range are more scattered and, consequently, the parameters of the defect distribution as evaluated from the fitting procedure are affected by large errors. Values of these parameters reported in Table I are only indicative. Due to the uncertainity in the analysis, it cannot be excluded that the positron traps at 750–850 °C are few vacancy clusters larger than V_4^*.

The distribution of positron traps, also after annealing, is always confined in the first 150 nm from the surface ($\bar{d}_1 = 85$ nm). Only the tails of the He and positron trap distributions overlap. The mean depth $\bar{d}_2$ of the near-to-surface distribution, has an almost constant value around 4 nm in the samples annealed in the 150–400 °C temperature range. Then it decreases at about 2 nm in the 450–650°C range.

3. Isochronal annealing of 2×10^{16} He cm^{-2} implanted samples

For annealing temperatures of 150–250 °C a decrease of V_2^* is observed; $\bar{d}_1$ moves slightly deeper (by about 10 nm) with respect to the as-implanted sample [Fig. 5(a)]. V_2^* increase as the annealing temperature is increased to 350°C; then they remain almost constant in the 350–450 °C temperature range [Fig. 5(b)]. In this temperature range $\bar{d}_1$ is about 100 nm.

From 500 °C the positron traps increase in size: V_3^*, V_4^*, V_6^* appear progressively. Our measured data in Fig. 6 suggest the absence of V_5^* defects. We cannot judge if this is a feature of our samples or if it is a general characteristic of defected Si. Starting from 600 °C, $\bar{d}_1$ moves progressively and reaches at 850 and 900°C, the mean depth of about 230 nm. At 800,850,900 °C, the traps are cavities (V_c) confined in a layer of about 30–40 nm centered around 230 nm [Fig. 5(d)]. We must note that the ΔS data at 700°C, already shows a small peak of defects at a depth around 150 nm, superimposed to the broader and larger distribution centered at 100 nm [see Fig. 5(c)]. This peak can be attributed to cavities; on the contrary, the tail of defects towards the surface has to be attributed to vacancy clusters of smaller size.

The final distribution of positron traps is centered in the same position as the He distribution after the implantation process (around 220 nm).

It is interesting to compare the PAS results shown in Fig. 5 with the ERD results in Fig. 1. In the 350–450 °C temperature range, where the positron trapping stops increasing, ERD evidences that the He content is almost constant. In the same temperature range there is also a decrease of the He desorption rate (see Fig. 2).

4. Comparison between the two series of samples

We can underline the following main differences and similarities between the evolution of the open volume defects as detected by PAS in the series implanted at low and high He dose.

(i) The samples implanted at LD show more positron traps in the region near the surface and the traps distribution is broader than in the HD series. A double-defect profile is needed to describe the trap's distribution.

(ii) Both series show that the number of V_1^* and V_2^* decreases in the 150–250 °C annealing temperature range, and that $\bar{d}_1$ increases at 250 °C with respect to the as-implanted samples.

(iii) At 300 °C, in both the series there is a sensible increase of $\bar{d}_1$ (from 50 to 80 and from 65 to 100 nm in the LD and HD series, respectively).

(iv) From 400 °C there is a diversification of open volume defects: in the series at LD only V_4^* appear, on the contrary in the HD series the open volume defects evolve from V_2^* to V_c with the progressive appearance of cluster of increasing size.

(v) In the 300–550 °C range the concentration of positron traps increases at about fixed $\bar{d}_1$ in the LD series. On the contrary, in the HD series, the concentration increases up to 350 °C, then remains constant up to 450 °C.

(vi) In the 600–900 °C range in the LD series the concentration of traps decreases. At 900 °C all the traps are annealed out. In the HD series, from 700 °C the concentration

decreases but the traps never disappear and their profile moves towards the bulk.

V. DISCUSSION

The present measurements show that the dynamics of the number of defects detected by PAS has three well-distinct stages in both series of samples (Figs. 4,5). The first at annealing temperatures lower than 250 °C in which open volume defects decrease, the second one from 250 to 650 °C, in which more and different open volume defects appear, the third one from 700 to 900 °C, in which cavities appear in the HD samples and open volume defects disappear in the LD samples. An explanation of the open-volume-defect dynamics is hardly separable from the behavior of He during the implantation process and its outdiffusion during the isochronal annealing as measured by TPD. Besides, the open volume defects interact with the damage due to the implantation, detected by RBSC. This damage is due to dislocations, He atoms, Si self-interstitials. These defects probably are connected to form extended defects as this damage starts to disappear at temperatures higher than 500 °C.

To our knowledge little information is available from the literature about vacancy clusters or vacancy complexes stabilized by other defects in Si. Different from He in metals, there are few experimental and theoretical studies about He in Si. The results achieved by these studies that useful for our discussion can be summarized as follows.

(a) Single vacancies are mobile well below room temperature in Si.[33]

(b) The annealing temperature of divacancies is around 250 °C;[34] other authors[27] have found an annealing temperature of about 300 °C for stabilized divacancies.

(c) It has been reported in electron paramagnetic resonance measurements that the annealing temperature of nonplanar tetravacancies is around 330 °C.[34]

(d) Alatalo *et al.*[35] have studied the very early stage of bubble formation in Si from first-principle molecular-dynamics calculation for He atoms in silicon. They have found that two He atoms in a perfect lattice tend to occupy adjacent T_d interstitial sites. The solution energy for the second He atom is 0.08 eV lower than that of a single He atom (0.88 eV). This energy can be regarded as the binding energy of the two atoms, therefore they are very stable at room temperature. From this result it is pointed out that the He bubble formation could start from clustering of an interstitial He. The He atom is found not to be trapped by single vacancies, excluding the possibility that the single vacancy is a nucleation center for He agglomeration.

(e) Helium was found to have the tendency to fill cavities.[36] From the point of view of positrons, filled cavities are passivated traps.[25]

The main results that we have obtained by a through comparison of the PAS data with the ERD, RBSC, and TPD measurements, are the following.

(1) Helium is shown to passivate also small open volume defects ($V_2^* - V_6^*$): this is demonstrated from the detection with PAS of vacancy complexes with character of vacancy cluster of increasing sizes as He outdiffuse by thermal treatments. Previous work[25] has demonstrated this passivation for large cavities only. TPD measurements (Fig. 2 and Sec. III) confirm that He is released with a distribution of activation energies, revealing the presence of heterogeneous traps. In addition the open-volume-defect distributions seen by PAS are confined in that region where the He concentration is lower.

(2) The number of open volume defects detected by PAS is very small in comparison with the implanted He dose and with the equivalent number of displaced Si atoms. Converting the number of open volume defects in Table I in a number of equivalent single vacancies we found that in the LD samples, as implanted and annealed at 250 °C, where the ERD and RBSC data are available,[21] the vacancies are about five times less than He and four times less than equivalent displaced Si atoms. The difference is more marked in the HD samples, about 70 times less than He and 500 times less than displaced Si. This relative difference decreases with the annealing temperature of the samples. This number of equivalent vacancies is evidently less than the expected number from the creation of Frenkel pairs during the implantation process. The small number of vacancy defects and the asymmetry in the behavior of the vacancy defects in the samples implanted at different He doses points out clearly that vacancies interact with He atoms and participate in the He clustering.

The interaction of vacancies with He atoms is twofold. From one side He can passivate the divacancies that are the only open volume defects expected to be left in the samples implanted at these He doses with this energy. On the other side mobile vacancies can be directly involved in the He clustering process. The dissolution of these He clusters during annealing is then responsible for the appearance of the vacancy clusters. The second point can be explained by the following considerations.

The He bubble formation process, according to the theoretical calculation,[35] is activated by the tendency of He to cluster. This clustering of He will be more effective in the region where the local concentration of He is higher.[10] In fact to accommodate more than four He atoms in the Si lattice it is necessary to create a vacancy. The energy needed to create a vacancy-interstitial pair (about 6 eV) can be achieved by the exothermic transfer of He from solid solution to the gas phase in the bubble. A rough estimate[14] shows that 30 He atoms at least are needed to form a bubble with a volume equivalent to four vacancies. On the other side a different mechanism should be called for where the density of He is lower (from the surface to about the He-projected range) and the number of vacancies produced by implantation is higher. It is more plausible that vacancies themselves contribute to the clustering process of He, decreasing the energy necessary to accommodate successive He atoms. Vacancies, in agreement with calculation,[35] would not be nucleation center for He clustering, but, due to their mobility, could be incorporated in the cluster during its formation. In this respect vacancies disappear just during the implantation process. At the end of the implantation process He is expected to be organized in agglomerates of different sizes, with the size of these clusters larger in the region of higher He concentration. In this way more vacancies are so left in the LD samples where the clustering process is less probable. The different maximum size of the vacancy clusters observed in the samples implanted at the two doses after He desorb-

tion (V_4^* in LD and V_6^* and V_c in HD) supports again the idea that the local density of He is responsible for the agglomeration process and for the disappearance of the vacancies during implantation.

(3) In the as-implanted sample and in the samples annealed up to 250°C the open defects detected by PAS are only those that survived He passivation. Their distribution is very near the surface where the He density is negligible. In the HD samples the mobile single vacancies are involved more efficiently in He clustering, and only the more stable V_2^* survive. The strong instability of V_1^* in the LD samples is well confirmed by the annealing at 150 °C in which about 2/3 of V_1^* disappear. In this first stage, according to the TPD and ERD measurements, there is a negligible loss of He from the samples, and RBSC measurements reported in Fig. 2 clearly show the decrease of displaced silicon atoms (this decrease is just in the near-surface region[13]). From the above consideration it can be deduced that during these first annealings the residual mobile He interstitial probably continues to contribute to the clustering process. The disappearance of V_1^* and of V_2^* can be ascribed to recombination with displaced silicon atoms, their migration and capturing by the He clusters that increase in size, and passivation by diffusing He atoms.

(4) In both series, starting from 250 °C, the concentration of V_2^* increases as He starts to outdiffuse (Fig. 2). At this stage all the V_1^* and the V_2^* survived after the implantation process have disappeared and the appearance of the new V_2^* and the appearance of vacancy complexes from 450 °C in the LD series and from 500 °C in the HD series can be explained with the depassivation of the open volume defects left by He detrapping and outdiffusion.

PAS measurements reveal that V_1^*,V_2^* and the other vacancy complexes must be stabilized by other defects or by He itself. In fact, as reported,[34] all vacancy clusters up to pentavacancies are expected to disappear at a temperature of 450 °C.

(5) In the LD series, V_4^* starts to disappear at 700 °C. At this temperature (see Fig. 1) all He has outdiffused. Conversely, in the HD series, the process evolves so that at 700 °C cavities are detected by PAS and TEM. At temperatures higher than 700 °C the desorption of He is almost total (Fig. 1) and TEM and PAS show an increase of cavity diameter and a decrease of cavity density due to a coalescence process.[10] PAS reveals also the disappearance of the small vacancy clusters from the surface down to 150 nm. They disappear above 700 °C (like in LD samples) leaving a Si lattice free from defects. The vacancies produced in the dissolution of these small clusters could migrate and be captured by the more stable bigger cavities.

VI. CONCLUSIONS

In conclusion we have followed with the PAS technique the evolution, as a function of isochronal annealing, of positron traps in implanted Si at two He doses. We have identified open volume defects with trapping characteristics ranging from single vacancy to hexavacancy. At the end of the annealing process we have identified cavities in the samples implanted at higher dose.

This dynamics shows that the He clustering process is highly favored by capturing of vacancies, especially in the region where the local concentration of He is lower. PAS measurements point out that, although the tendency of He to coalesce is the driving force in He bubble formation, any model or theoretical calculation must take into account the interaction of He with vacancies during the implantation and the first annealing stages. From the appearance of vacancy clusters of different size during He outdiffusion, it is evident that He, like H,[37] passivates also small voids and not only cavities. The revealed vacancy complexes, due to the high annealing temperature, are found to be very stable and stabilized by He or He-related defects.

ACKNOWLEDGMENTS

One of us (N.T.) thanks the Istituto Nazionale Fisica per Materia (INFM) for financial support. The authors thank G. Calzolari and C. Nobili (Universita' di Modena) for helpful discussions. This work was partially supported by the Ministero dell'Universita' e della Ricerca Scientifica e Tecnologica (MURST).

APPENDIX: MODELLING OF PAS RESULTS

We have determined the parameters that characterize the open-volume-defect distributions (N_{nv},$\bar{d}_1$,$\bar{d}_2$) and the nature of the open volume defects (S_d), by a best fit of the S vs E experimental curves. We have adopted for the fitting procedure the diffusion model.[23,37] In this model the parameter is expressed as a linear combination of three terms:[19]

$$S(E)=S_s f_s(E)+S_b f_b(E)+S_d f_d(E), \tag{A1}$$

where $f_s(E)$,$f_b(E)$,$f_d(E)$ are the positron annihilation probabilities at the surface, in the bulk, and in the defects respectively. S_s,S_b,S_d are the characteristic values of S for positrons annihilating at the surface, in the bulk, and in the defects, respectively. The energy- (depth) dependent $f_s(E)$,$f_b(E)$,$f_d(E)$ probabilities are related to the stationary density $n(x,E)$ of thermal positrons, at incident positron energy E and at depth x, by the equations.

$$f_b(E)=\lambda\int_0^\infty n(x,E)dx, \tag{A2}$$

$$f_s(E)=D_+\left[\frac{dn(x,E)}{dx}\right]_{x=0}, \tag{A3}$$

$$f_d(E)=\nu\int_0^\infty C(x)n(x,E)dx, \tag{A4}$$

where λ is the bulk annihilation rate in c-Si [for which we have accepted the theoretical value $\lambda=(221\ \text{ps})^{-1}$ (Ref. 15)], D_+ is the positron diffusion constant, ν,$C(x)$ are the specific trapping rate per unit defect concentration and the function describing the profile of positron traps, respectively. The specific trapping rate is related to the defect concentration c_d (defects per unit area per host atom) through the equation

$$\nu=c_d\nu_d, \tag{A5}$$

where ν_d is the characteristic trapping rate of the defect.

The positron density $n(x,E)$ is the solution of the diffusion equation

$$D_+ \frac{d^2 n(x,E)}{dx^2} - \frac{d}{dx}[\mu_+ E_x n(x,E)] - [\lambda + \nu C(x)]n(x,E) + P(x,E) = 0. \quad \text{(A6)}$$

μ_+ is the positron mobility, related to the diffusion constant and to the thermal energy $k_b T$ by the Einstein equation $\mu_+ = eD_+/k_b T$ (e is the electron charge and k_b the Boltzman constant). E_x is the electric field in the direction of the x axis. As it is well known in p-silicon samples an electric field associated to the band bending near the surface pushes the positron away from the surface. $P(x,E)$, the positron implantation profile, is the positron density profile at the end of the thermalization process. As the positron-implantation profile we have used the Makhov function,[38]

$$P(x,E) = -\frac{d}{dx}\exp\left[-\left(\frac{x}{x_0}\right)^m\right], \quad \text{(A7)}$$

where $m=1.9$ and x_0 is related to the mean implantation depth by means of the equation

$$\bar{x} = 0.887 x_0 = (A/\rho)[E(keV)]^n \quad \text{(A8)}$$

with the density of silicon ρ=2.33 g/cm^3. A and n are two parameters characteristic of the investigated material. The solution of Eq. (A6) has been obtained by a numerical routine.[39]

Reference sample

As a first step in the application of the diffusion model, the diffusion constant D_+, the surface electric field E_x, and the two parameters A and n must be evaluated. This has been done, as usual, by fitting an S vs E curve of an undefected sample with Eq. (A6): in this case $\nu=0$. These parameters are to be evaluated with care because they will affect directly the determination of the depth reported in Table I.[37] A critical point is the evaluation of the surface electric field.[37] We have found that the surface of our samples was modified by the implantation process. All of the as-implanted samples and the annealed samples of the two series have shown an S_s value close to 0.92 (see for example Fig. 3). This value is lower than the S_s value of about 0.95 measured for a $p(100)$ sample before implantation. In Fig. 7 we have reported the S measurements for a virgin sample $p(100)$(1.7–2.5 cm) and for a $p(100)$ (1.7–2.5 cm) sample implanted at LD and annealed at 900 °C. This last sample appears as a defect-free crystalline sample as analyzed by RBSC, ERD, and PAS. Therefore, the two samples are expected to have the same bulk properties (the same D_+, A, n). In our analysis we have assumed that the difference in the S curves of Fig. 7 can be ascribed to a change of the surface electric field. Consequently we have fitted the data of the two samples reported in Fig. 7, with E_x, D_+, A, n as free best fit parameters but with the constraint that on D_+, A, n shall be the same for the two samples. The best fit values for A, n, and D_+ have been found to be $A=3.5$ g/cm^2 and $n=1.7$, and $D_+=2.1 \pm 0.2$ cm^2/s [D_+ is related to the diffusion length through $L_+ = (D_+/\lambda)^{0.5} = 215 \pm 10$ nm]. The surface electric field has been taken with the linear dependence on x predicted by the Poisson equation in the constant carrier-density approximation.[39] The surface-bulk potential difference V associated with the surface electric field has been found to be $V=0$ for the annealed sample and $V=67$ mV for the virgin sample. The results found with the above procedure for the annealed sample have been used in the analysis of all the samples of the two series. The mean depth distribution of cavities found with this PAS analysis in HD implanted samples and annealed at 800–900 °C is in perfect agreement with TEM measurements. This has to be considered as *a posteriori* confirmation of the correctness of our evaluation.

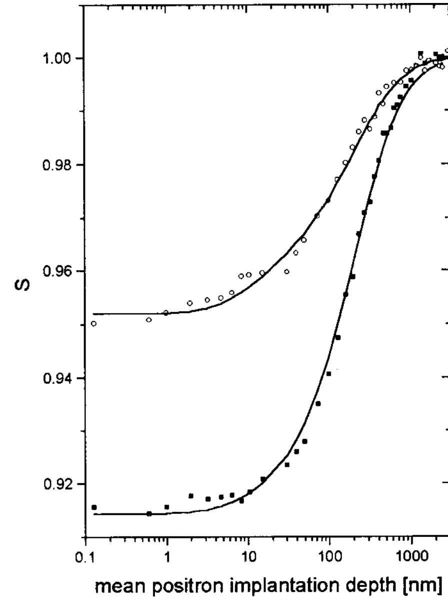

FIG. 7. Parameter vs mean positron implantation depth for a $p(100)$ sample (open circles) and a LD sample annealed at 900 °C (full squares).

As-implanted and annealed samples

The measured S vs E curves of the as-implanted and annealed samples have been fitted with Eq. (A6) in which the specific trapping rate ν and the defect profile $C(x)$ were kept as a free parameter and an estimating function, respectively. As an estimate for the defect profile a derivative of a Gaussian was chosen:

$$C(x) = \frac{1.573}{\bar{d}} \frac{x}{\bar{d}} \exp\left[-\left(\frac{0.887x}{\bar{d}}\right)^2\right]. \quad \text{(A9)}$$

The constants in Eq. (A9) ensure the condition $\int_0^\infty C(x)dx = 1$, $\int_0^\infty xC(x)dx = \bar{d}$. $\bar{d}$ is the mean depth of the defect density profile. With this function it was possible to fit the samples of the 2×10^{16} He cm^{-2} series from the as-implanted sample to the sample annealed at 550 °C. In this case the free fitting parameters were $\bar{d}$ (in Table I as $\bar{d}_1$) and the specific trapping rate ν.

All the samples in the LD series and the samples of the HD series annealed in the 600–750 °C temperature range present a shoulder of defects near to the surface (see Figs. 4 and 5). To obtain a good quality fit, it was necessary to use

an estimate function, which is the sum of two equations like Eq. (A9). The free fitting parameters were $S_d, S_s, \bar{d}_1, \bar{d}_2$, and the two trapping rates were ν_1, ν_2. The S_s parameter of the surface was varying from 0.90 to 0.922 and from 0.896 to 0.917 in the low and high dose samples, respectively.

In the case of the samples of the HD series annealed in the 800–900 °C temperature range, no defects were observed in the region from the surface down to 150 nm. To obtain a good quality fit to the data a Gaussian was adopted as the estimate function:

$$C(x)=\frac{1}{\sqrt{2\pi}}\frac{1}{\sigma}\exp\left[-\frac{(x-\bar{d}_1)^2}{2\sigma^2}\right], \quad \text{(A10)}$$

where 2.34σ is the full width at half-maximum.

The errors on the best fit parameters have been estimated in correspondence with an increase of $1/n$ of the square of the variance of the fit, where n is the number of degrees of freedom.

The best fit procedure, applied to the S vs E curves of some samples annealed at temperatures higher than 500 °C, failed in determining accurately the S_d parameter. This fact was due to the interrelation between the specific trapping rate and the S_d best fit parameters. A decrease in the specific trapping rate is compensated by an increase in S_d, making it difficult to find out its upper limit. The method proposed by Clement *et al.*[24] has been adopted to check the S_d parameters as evaluated by the fit procedure and to evaluate the S_d parameters in the uncertain cases. In this method, based on the linearity properties of the shape and the wing parameters, the $S(E)$ and $W(E)$ parameters are plotted as a trajectory in the S-W plane. As an example, Fig. 8 shows the S-W plot for a sample implanted at HD and annealed at 600 °C. Two straight lines are easily identified starting from the surface (S values close to 0.92) and from the bulk (S values close to 1.0). The intersection of these lines yields the characteristic S_d and W_d parameters of the defected layer. The uncertainty limits on the two parameters have been evaluated from the variance in the slope of the two straight lines. In the case of Fig. 8 the second line has been determined by a linear fit to the measured points in the 20–25-keV energy range: here

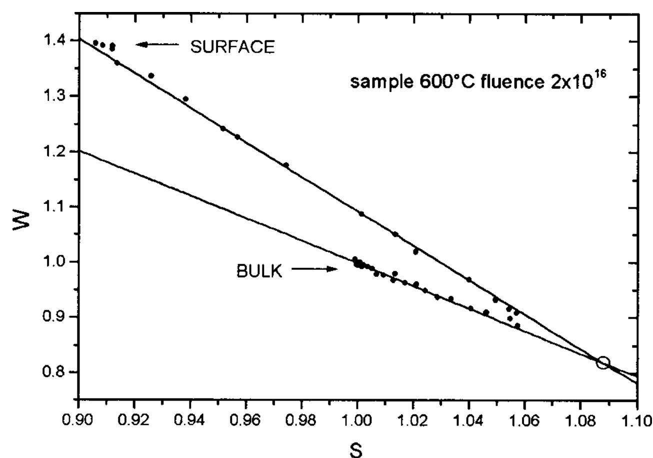

FIG. 8. W vs S curve for a HD sample annealed at 600 °C. The lines are best fits as discussed in the Appendix.

the probability for a positron to annihilate at the surface is negligible. For the first line, the points in the 8–12-keV energy range have been used: here the probability of annihilation in the bulk is negligible. These energy intervals were chosen by crosschecking the f_d and f_s values with the diffusion equation.

In the present work this method has given the same values of S_d as obtained by fitting the diffusion equation to the measured curves of all the samples annealed in the 400–550 °C temperature range. The method has given poor results in the analysis of those samples in which the increase of the measured S vs E parameter was not so pronounced (as-implanted, 150–300 °C temperature range samples). The S vs W method performed better than the diffusion equation for all the samples annealed at temperatures higher than 600 °C. In the samples in which there was a decrease of positron traps, the S_d value was fixed. In particular, the S_d value of 1.112, found for the HD implanted sample and annealed at 700 °C, was kept fixed to analyze the samples annealed at a higher temperature. $S_d=1.02$ and $S_d=1.0376$ were kept fixed in the analysis of the samples annealed at 150–200 °C, implanted at LD and HD doses respectively (see Fig. 6 and Table I).

*Electronic address: BRUSA@science.unitn.it

[1] *Positron Spectroscopy of Solids*, edited by A. Dupasquier and A. P. Mills, Jr. (North-Holland, Amsterdam, 1995).
[2] P. Asoka-Kumar, K.G. Lynn, and D.O. Welch, J. Appl. Phys. **76**, 4935 (1994).
[3] C. Corbel and P. Hautojärvi, in *Positron Spectroscopy of Solids* (Ref. 1), p. 533.
[4] C.C. Griffioen, J.H. Evans, P.C. De Jong, and A. Van Veen, Nucl. Instrum. Methods Phys. Res. B **27**, 417 (1987).
[5] J.H. Evans, A. Van Veen, and C.C. Griffioen, Nucl. Instrum. Methods Phys. Res. B **28**, 360 (1987).
[6] R. Siegele, G.C. Weatherly, H.K. Haugen, D.J. Lockwood, and L.M. Howe, Appl. Phys. Lett. **66**, 1319 (1995).
[7] C.H. Seager, S.M. Myers, R.A. Anderson, W.L. Warren, and D.M. Follstaedt, Phys. Rev. B **50**, 2458 (1994).
[8] D.J. Eaglesham, A.E. White, L.C. Feldman, N. Moriya, and D.C. Jacobson, Phys. Rev. Lett. **70**, 1643 (1993).
[9] S.M. Myers, D.M. Follstaedt, H.J. Stein, and W.R. Wampler, Phys. Rev. B **45**, 3914 (1992).
[10] V. Raineri, P.G. Fallica, G. Pecorella, A. Battaglia, M. Barbagallo, and S.U. Campisano, J. Appl. Phys. **78**, 3727 (1995).
[11] V. Raineri and M. Saggio, Appl. Phys. Lett. **71**, 1673 (1997).
[12] R.S. Brusa, G.P. Karwasz, N. Tiengo, A. Zecca, F. Corni, G. Calzolari, and C. Nobili, J. Appl. Phys. **85**, 2390 (1999).
[13] R. Tonini, F. Corni, S. Fabbroni, G. Ottaviani, and G. Cerofolini, J. Appl. Phys. **84**, 4802 (1998).
[14] F. Corni, C. Nobili, G. Ottaviani, R. Tonini, G. Calzolari, G.F. Cerofolini, and G. Queirolo, Phys. Rev. B **56**, 7331 (1997).
[15] M. Hakala, M.J. Puska, and R.M. Nieminen, Phys. Rev. B **57**, 7621 (1998).
[16] J.F. Ziegler, J.P. Biersack, and U. Littmark, *The Stopping and Range of Ions in Solids* (Pergamon, New York, 1985).
[17] R.S. Brusa, G.P. Karwasz, M. Bettonte, and A. Zecca, in *Slow Positron Beam Techniques for Solids and Surfaces*, edited by

W.B. Waeber, M. Shi, and A.A. Manuel (Elsevier, Amsterdam, 1997); Appl. Surf. Sci. **116**, 59 (1997).

[18] A. Zecca, M. Bettonte, J. Paridaens, G.P. Karwasz, and R.S. Brusa, Meas. Sci. Technol. **9**, 1 (1998).

[19] P. Hautojärvi and C. Corbel, in *Positron Spectroscopy of Solids* (Ref. 1), p. 491.

[20] R.S. Brusa, M. Duarte Naia, R. Grisenti and A. Zecca, in *Positron Annihilation*, edited by Z. Kajcsos and C. Szeles (Trans. Tech. Aedermannsdorf, Switzerland 1992); Mater. Sci. Forum **105-110**, 1853 (1991).

[21] F. Corni, G. Calzolari, S. Fabbroni, C. Nobili, G. Ottaviani, R. Tonini, G.F. Cerofolini, D. Leone, M. Servidori, R.S. Brusa, G.P. Karwasz, N. Tiengo, and A. Zecca, J. Appl. Phys. **85**, 1401 (1999).

[22] D.M. Follstaedt, Appl. Phys. Lett. **62**, 1116 (1993).

[23] A. Dupasquier and G. Ottaviani, in *Positron Spectroscopy of Solids* (Ref. 1), p. 581.

[24] M. Clement, J.M.M. de Nijs, P. Balk, H. Shut, and A. van Veen, J. Appl. Phys. **79**, 9029 (1996).

[25] R.A. Hakvoort, A. van Veen, P.E. Mijnarends, and H. Shut, in *Slow Positron Beam Techniques for Solids and Surfaces*, edited by M. Doyama, T. Akahane, and M. Fujinami (Elsevier, Amsterdam, 1995); Appl. Surf. Sci. **85**, 271 (1995).

[26] J. Keinonen, M. Hautala, E. Rauhala, V. Karttunen, J. Risnen, J. Lahtinen, A. Vehanen, E. Punkka, and P. Hautojärvi, Phys. Rev. B **37**, 8269 (1988).

[27] P.J. Simpson, M. Vos, I.V. Mitchell, C. Wu, and P.J. Schultz, Phys. Rev. B **44**, 12 180 (1991).

[28] H. Kauppinen, C. Corbel, K. Skog, K. Saarinen, T. Laine, P. Hautojärvi, P. Desgardin, and E. Ntsoenzok, Phys. Rev. B **55**, 9598 (1997).

[29] V. Avalos, and S. Dannefaer, Phys. Rev. B **54**, 1724 (1996).

[30] G.D. Watkins and J.W. Corbett, Phys. Rev. **121**, 1001 (1961).

[31] R.M. Nieminen and J. Laakkonen, Appl. Phys. **20**, 181 (1979).

[32] A. Kawasuso, M. Hasegawa, M. Suezawa, S. Yamaguchi, and K. Sumino, Jpn. J. Appl. Phys., Part 1 **34**, 2197 (1995).

[33] G.D. Watkins and J.W. Corbett, Phys. Rev. **138**, A543 (1965).

[34] J.W. Corbett, J.P. Karins, and T.Y. Tan, Nucl. Instrum. Methods **182/183**, 457 (1981).

[35] M. Alatalo, M.J. Puska, and R.M. Nieminen, Phys. Rev. B **46**, 12 806 (1992).

[36] A. van Veen, A.H. Reader, D.J. Gravesteijn, and A.A. van Gorkum, Thin Solid Films **241**, 206 (1993).

[37] R.S. Brusa, M. Duarte Naia, A. Zecca, C. Nobili, G. Ottaviani, R. Tonini, and A. Dupasquier, Phys. Rev. B **49**, 7271 (1994).

[38] S. Valkealahti and R.M. Nieminen, Appl. Phys. A: Solids Surf. **35**, 51 (1984).

[39] A. Dupasquier and L. Quartapelle, Appl. Phys. A: Solids Surf. **44**, 239 (1987).